Desalination and Water Treatment
www.deswater.com

doi: 10.5004/dwt.2021.27836

242 (2021) 94–99
December

Influence of PEG on the properties of gadolinium titanate photocatalyst for RBR X-3B degradation

Jiaying Zhang, Wenjie Zhang*, Jiao Yang

School of Environmental and Chemical Engineering, Shenyang Ligong University, Shenyang 110159, China, emails: wjzhang@aliyun.com (W. Zhang), 3060781822@qq.com (J. Zhang), 1206329565@qq.com (J. Yang)

Received 1 June 2021; Accepted 25 September 2021

ABSTRACT

Polyethylene glycol (PEG) acted as a pore-forming agent in a sol–gel route to synthesize porous gadolinium titanate. The influences of PEG on the composition, surface morphology and activity of gadolinium titanate were studied. Pyrochlore structured $Gd_2Ti_2O_7$ was produced in the materials, while $Gd_2Ti_2O_7$ crystals grew slowly in GTO(PEG) after using PEG in the precursor. The Fourier-transform infrared spectroscopy absorption intensity of the Gd-O bond of GTO(PEG) was strengthened. Gadolinium of GTO was in Gd^{3+} oxidation state, and titanium of GTO was in Ti^{4+} oxidation state. The calcination process resulted in large $Gd_2Ti_2O_7$ particles without porous structure, while the porous structure was formed in GTO(PEG) after removing PEG during calcination. The degradation efficiency of GTO was much smaller than the degradation efficiency of GTO(PEG). In the presence of GTO(PEG), RBR X-3B solution was fully decolorized after 100 min, but total organic carbon removal efficiency was 79.4% after 180 min. The degradation efficiency of GTO(PEG) decreased from 47.5% to 30.3% after five degradation cycles.

Keywords: $Gd_2Ti_2O_7$; Photocatalysis; Sol–gel; Pore-forming agent; Degradation

1. Introduction

Toxic organic substances in industrial wastewater are not allowed to discharge. However, since microorganisms cannot survive in toxic wastewater, the biochemical technique is not applied for toxic wastewater treatment [1–3]. The photocatalytic technique is an advanced oxidation technique, and it was applied to oxidize most kinds of organic pollutants [4–9]. The photocatalytic oxidation process can usually lead to the thorough mineralization of organic substances [10,11].

The development of photocatalytic material is an important research focus. Although a lot of work concerned the progress of titania, novel and powerful photocatalytic materials, for example, $ZnWO_4$, were always interesting [12–15]. Developing photocatalytic material is a titanate, which has wide application in organic substance removal [16–20]. High-temperature calcination is necessary for titanate crystallization, and therefore, the as-prepared titanate normally contains large particles as a result of crystal aggregation. Nevertheless, these large titanate particles usually do not have good activity on organic substance degradation. Since a pore-forming agent was successfully used in the preparation of porous titania [21], it would be interesting to utilize a pore-forming agent to prepare titanate.

Polyethylene glycol (PEG) acted as a pore-forming agent in a sol–gel process to prepare gadolinium titanate in this work. Macromolecular PEG provided hydrolysis centers for tetrabutyl titanates in the precursor. Pores were left in gadolinium titanate after removing PEG during calcination, leading to a loose and porous structure in gadolinium titanate. The influences of PEG on the composition, surface morphology and photocatalytic activity of gadolinium titanate were studied. RBR X-3B azo dye was used as a probe reactant in the photocatalytic oxidation process.

* Corresponding author.

2. Experimental methods

2.1. Gadolinium titanate preparation

PEG was the pore-forming agent in the sol–gel route. PEG (0.001 mol) and tetrabutyl titanate (0.0025 mol) were dissolved in ethanol (8 mL) to prepare solution X. $Gd(NO_3)_3{\cdot}6H_2O$ (0.0025 mol) was dissolved in the mixture of deionized water (10 mL) and acetic acid (8 mL) to prepare solution Y. Solution X and solution Y were stirred together to prepare a transparent sol. Sol–gel transformation was accomplished after 60 min. The gel was calcined for 3 h at 800°C to produce gadolinium titanate. GTO was referred to the sample prepared without PEG, and GTO(PEG) was referred to the sample prepared using PEG.

2.2. Characterization of the materials

An X-ray diffractometer was applied to the materials (D8, λ = 0.15416 nm (Cu Kα)). The materials were deposited with a gold layer to take the images on a scanning electron microscope (QUANTA250). The X-ray photoelectron (XPS) spectra were obtained on an X-ray photoelectron spectroscopy (ESCALAB 250Xi). The Fourier-transform infrared spectroscopy (FT-IR) spectrum was obtained using a Frontier spectrometer. The bandgap energy of the material was determined on a UV-Vis spectrometer (scanning speed 480 nm/min, LAMBDA 35).

2.3. Photocatalytic activity measurement

RBR X-3B ($C_{19}H_{10}Cl_2N_6Na_2O_7S_3$) was used to determine the activity of gadolinium titanate. 30 mg of gadolinium titanate powders and 50 mL of dye solution (30 mg/L) were stirred in the dark until the dye concentration was stable. A 20 W UV lamp (253.7 nm) was turned on to start the photocatalytic reaction. RBR X-3B concentration was determined using a 721E spectrophotometer. Total organic carbon (TOC) analysis was obtained using an Analytikjena multi N/C 3100 analyzer.

3. Results and discussion

3.1. Material composition

The crystallization of gadolinium titanate in the samples can be seen in Fig. 1. The only crystallized substance in the samples was $Gd_2Ti_2O_7$ in the cubic system. The diffraction pattern of gadolinium titanate, accompanied by the preferred orientation, was as same as the pattern in JCPDS 54-0180. The diffraction patterns of GTO and GTO(PEG) samples were almost the same, showing a solely pyrochlore structured $Gd_2Ti_2O_7$ phase. Impurity and other phases of gadolinium titanate were not shown in the X-ray diffraction patterns. Although PEG did not influence the gadolinium titanate phase, the addition of a pore-forming agent did result in a slight decrease in diffraction intensity. The Scherrer formula $L = K\lambda/(\beta\cos\theta)$ was used to calculate the crystallite size of pyrochlore $Gd_2Ti_2O_7$ [22]. The crystallite size of GTO was 38.8 nm, while the crystallite size of GTO(PEG) was 28.6 nm. $Gd_2Ti_2O_7$ crystals grew slowly in GTO(PEG) after using PEG.

The functional groups in GTO and GTO(PEG) can be observed in the FT-IR spectra, as presented in Fig. 2. Surface adsorbed O–H groups had absorptions around 3,440 and 1,645 cm^{-1}. Hydroxyl groups could be utilized to produce hydroxyl radicals, so surface adsorbed O–H was a common characteristic of the photocatalyst. The materials were calcined for 3 h at 800°C to produce gadolinium titanate. However, organic substances were not thoroughly burnt out and the organic residues had absorptions at 2,923 and 2,851 cm^{-1}. The absorptions at 1,747 and 1,468 cm^{-1} were also related to the remaining organic resides, that is, C=O and C–H groups. The absorptions at 555 and 451 cm^{-1} were due to Gd-O bond, representing stretching vibration and bending vibration of Gd-O bond [23]. The absorption intensity of Gd-O bond in GTO(PEG) was strengthened.

The chemical environments of gadolinium, oxygen and titanium in GTO and GTO(PEG) are ascertained from the XPS spectra. As illustrated in Fig. 3a, electron binding

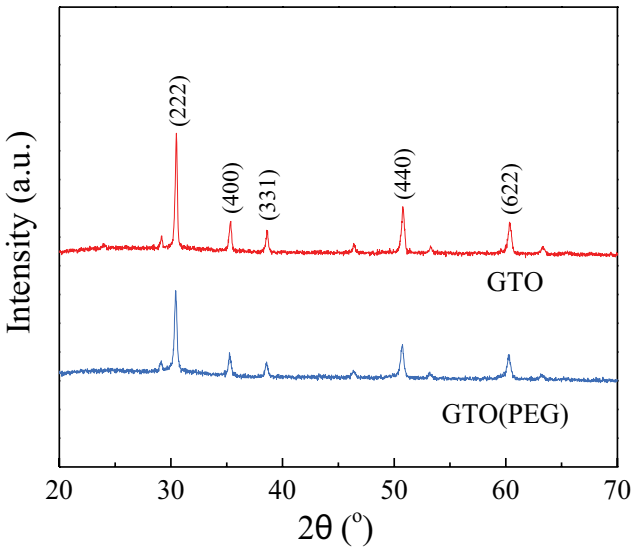

Fig. 1. X-ray diffraction patterns of GTO and GTO(PEG).

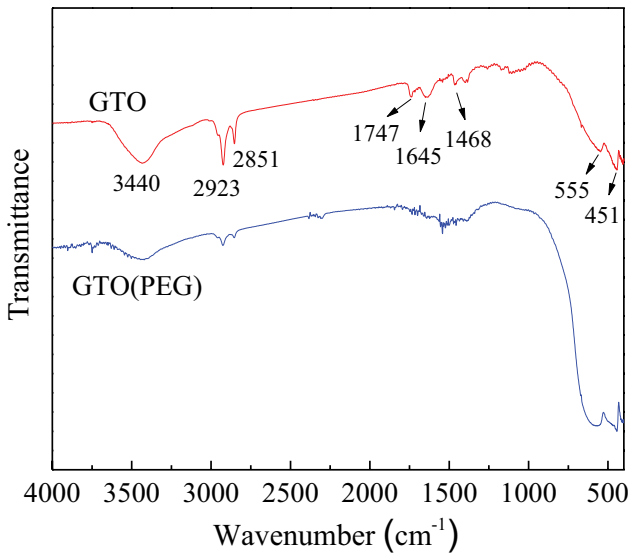

Fig. 2. FT-IR spectra of GTO and GTO(PEG).

energies at 1,219.6 and 1,187.2 eV were for $Gd3d_{3/2}$ and $Gd3d_{5/2}$ orbitals of GTO, respectively. $Gd3d_{5/2}$ orbital electrons had a weak shake-up peak at 1,197.1 eV. Gadolinium in GTO was in Gd^{3+} oxidation state [24]. At the same time, electron binding energies of $Gd3d_{3/2}$ and $Gd3d_{5/2}$ orbitals of GTO(PEG) moved to low energy end. Gadolinium ion of GTO(PEG) was less positive than Gd^{3+} ion of GTO.

As shown in Fig. 3b, O1s electrons had two different states. 531.5 eV corresponded to O–H groups adsorbed on the material surface, and 529.6 eV was related to Gd-O bond of GTO [25]. There was only a minor decrease of O1s electron binding energy after using PEG. The Ti2p XPS spectra of GTO and GTO(PEG) samples were almost the same, as presented in Fig. 3c. Binding energy of 464.1 eV was for $Ti2p_{1/2}$ electrons and the energy of 458.3 eV was for $Ti2p_{3/2}$ electrons. Titanium of GTO and GTO(PEG) was in Ti^{4+} oxidation state.

3.2. Surface morphologies of GTO and GTO(PEG)

The influence of PEG on the morphology of the material is presented in Fig. 4. High temperature calcination process was necessary for crystallization of pyrochlore structured $Gd_2Ti_2O_7$. Nevertheless, strong aggregation tendency of $Gd_2Ti_2O_7$ crystals led to very large particles in the size as large as tens of micrometers. GTO did not have apparent porous structure in the large particles with smooth surface. Tetrabutyl titanate was hydrolyzed to produce Ti–OH, and Ti–OH groups were connected to form an infinitive Ti–OH network in the gel. The calcination process resulted in large $Gd_2Ti_2O_7$ particles without porous structure. The hydrolysis mechanism might be different in PEG-mediated sol–gel process. Tetrabutyl titanate was distributed on macromolecular PEG to inhibit Ti–OH network extension, proven by shrinking crystallite size of $Gd_2Ti_2O_7$. Porous structure was formed in GTO(PEG) after removing PEG during calcination.

3.3. Bandgap position

Fig. 5 schematically illustrates electron excitation in GTO(PEG). The bandgap E_g of GTO(PEG) was 3.64 eV, obtained from diffuse reflectance spectrum. The conduction band potential (E_{CB}) and the valence band potential (E_{VB}) were –0.68 and 2.96 V, calculated from $E_{CB} = X - E^C - 1/2E_g$ and $E_{VB} = E_{CB} + E_g$ [26]. Due to positive E_{CB} and negative E_{VB} of GTO(PEG), $H_2O(OH^-)/{}^{\bullet}OH$ and $O_2/O_2^{-\bullet}$ reactions can occur

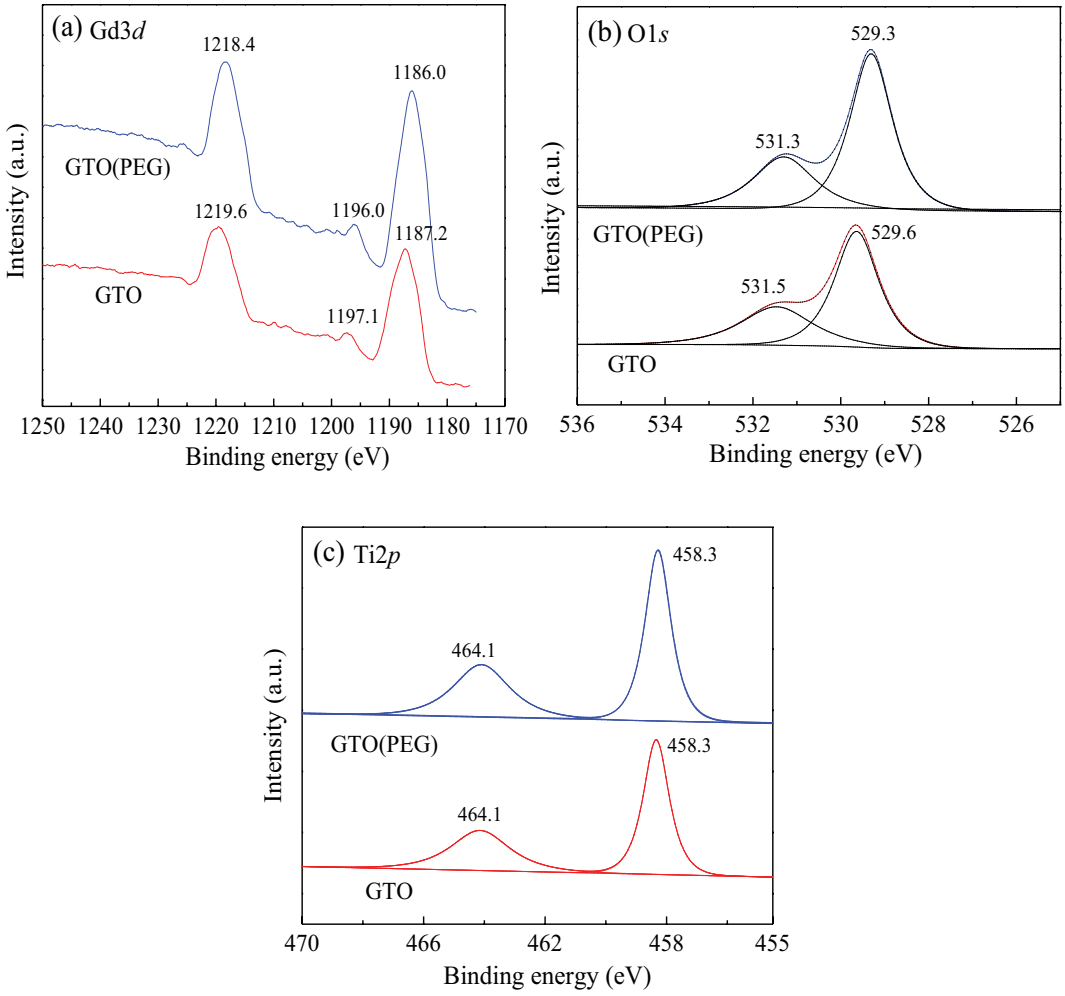

Fig. 3. XPS spectra of GTO and GTO(PEG) samples.

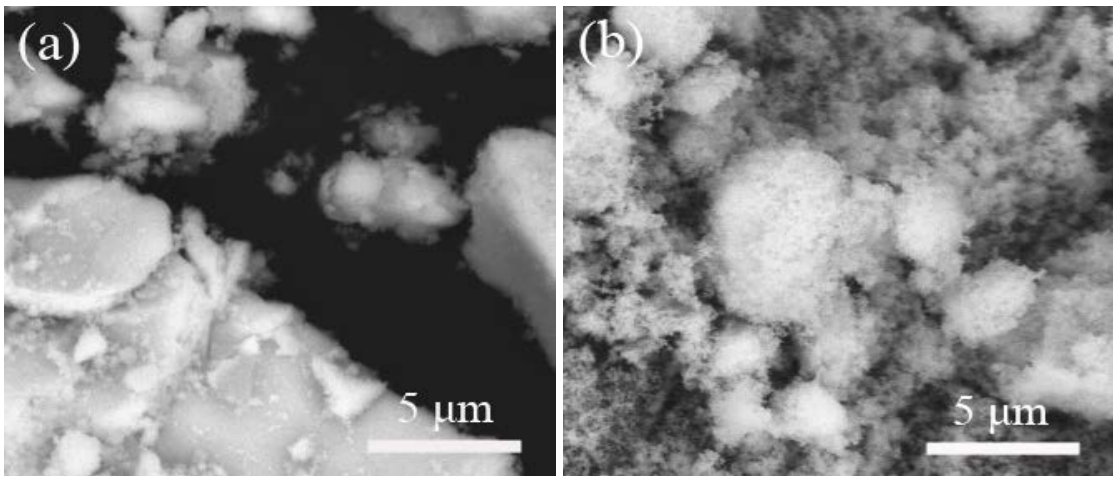

Fig. 4. Scanning electron microscopy surface morphologies of (a) GTO and (b) GTO(PEG) samples.

on GTO(PEG). These radicals will be used in the degradation process.

3.4. RBR X-3B removal

Photocatalytic degradation of RBR X-3B on GTO and GTO(PEG) in the prolonged reaction is presented in Fig. 6. Fig. 6a gives the reduced RBR X-3B concentration in the solution during degradation. RBR X-3B solution was nearly fully decolorized after 100 min in the presence of GTO(PEG), while the degradation efficiency was much slower in the solution containing GTO. The remaining RBR X-3B concentration was 68.1% of the initial RBR X-3B concentration after 100 min reaction in the presence of GTO.

Organic carbon in the solution was continuously removed during the degradation reaction, as illustrated in Fig. 6b. Organic carbon removal efficiency depended on the activity of the photocatalyst. However, TOC removal was slower than decoloration of the solution. For example, in the presence of GTO(PEG), the solution was nearly fully decolorized after 100 min, but TOC removal efficiency was 79.4% after 180 min. The breaking up of chromophore in the dye was much faster than mineralization of the intermediates.

Fig. 7 shows the reusability of GTO and GTO(PEG) in five photocatalytic degradation cycles. The reaction time of each cycle was 30 min. After a degradation cycle was finished, a volume of stock dye solution was replenished into the solution before starting the next degradation cycle. Degradation efficiency of GTO(PEG) decreased from 47.5% to 30.3% after five degradation cycles, while degradation efficiency of GTO decreased from 28.8% to 16.2% after five degradation cycles. The reduced degradation efficiency might be due to inactivation of the material, but the loss of fine particles at sampling might also be responsible for the reduced efficiency.

4. Conclusions

PEG was used as pore forming agent in the sol–gel route to prepare gadolinium titanate. PEG inhibited $Gd_2Ti_2O_7$ crystals growth in GTO(PEG). The functional groups in GTO and GTO(PEG) were observed in the FT-IR

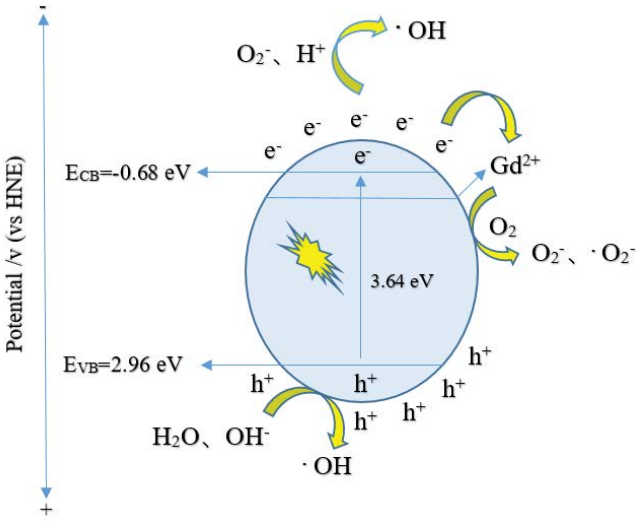

Fig. 5. Schematic illustration of electron excitation in GTO(PEG). The bandgap E_g of GTO(PEG) was 3.64 eV.

spectra. Gadolinium of GTO was in Gd^{3+} oxidation state, and gadolinium ion of GTO(PEG) was less positive than Gd^{3+} ion of GTO. Porous structure was formed in GTO(PEG) after removing PEG during calcination. GTO(PEG) showed an apparently improved photocatalytic activity than GTO. Decomposition of chromophore in RBR X-3B dye was much faster than mineralization of the intermediates. Degradation efficiency of GTO(PEG) decreased from 47.5% to 30.3% after five degradation cycles.

Competing interests

The authors have no relevant financial or non-financial interests to disclose.

Funding info

This work was supported by Construction project of research innovation group of Shenyang Ligong University (SYLUTD202108).

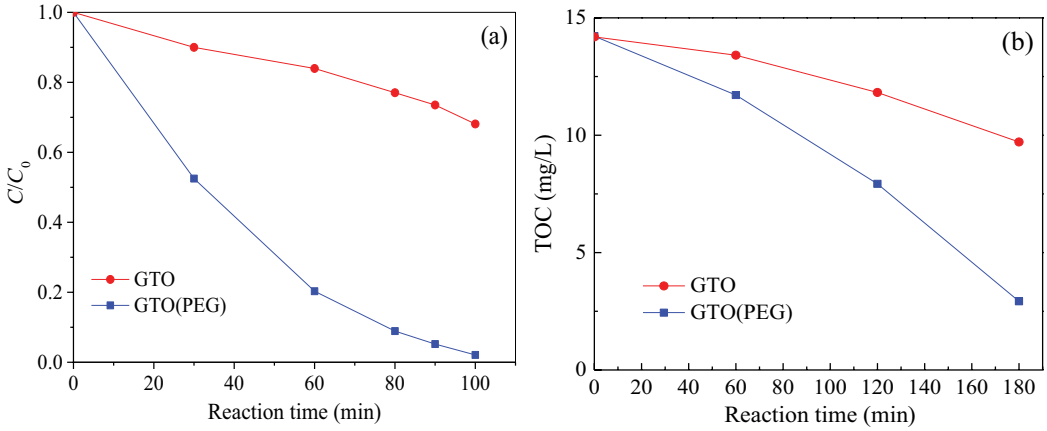

Fig. 6. (a) Photocatalytic degradation of RBR X-3B on GTO and GTO(PEG) and (b) TOC removal of the dye solution.

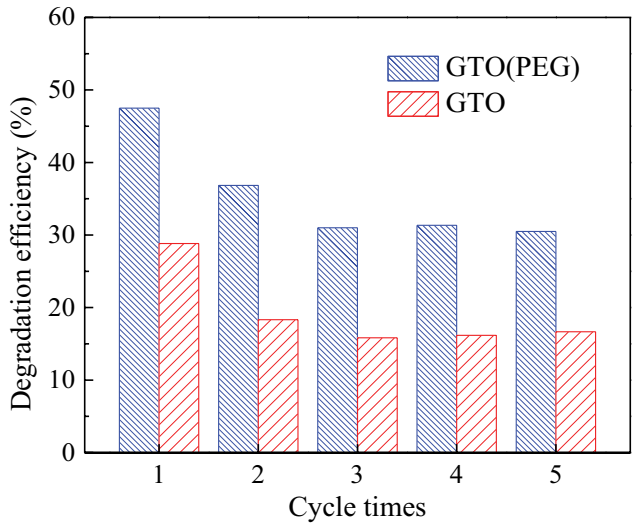

Fig. 7. Reusability of GTO and GTO(PEG) for RBR X-3B degradation.

Author contribution

Jiaying Zhang: Data curation, Methodology, Investigation.

Wenjie Zhang: Supervision, Writing- Reviewing and Editing.

Jiao Yang: Data curation, Investigation.

Consent to participate (Ethics)

All authors agree to the submission. The submitted paper has not been published previously and is not currently submitted for review to any other journal and will not be submitted elsewhere before a decision is made by this journal.

Acknowledgements

None.

References

[1] D. Barceló, B. Žonja, A. Ginebreda, Toxicity tests in wastewater and drinking water treatment processes: a complementary assessment tool to be on your radar, J. Environ. Chem. Eng., 8 (2020) 104262, doi: 10.1016/j.jece.2020.104262.

[2] H.B. Lu, Y. Yu, Y.X. Zhou, F. Xing, A quantitative evaluation method for wastewater toxicity based on a microbial fuel cell, Ecotoxicol. Environ. Saf., 183 (2019) 109589, doi: 10.1016/j.ecoenv.2019.109589.

[3] W.T. Zhao, Q. Sui, X. Huang, Removal and fate of polycyclic aromatic hydrocarbons in a hybrid anaerobic–anoxic–oxic process for highly toxic coke wastewater treatment, Sci. Total Environ., 635 (2018) 716–724.

[4] J. Zan, H. Song, S.Y. Zuo, X.R. Chen, D.S. Xia, D.Y. Li, MIL-53(Fe)-derived Fe_2O_3 with oxygen vacancy as Fenton-like photocatalysts for the elimination of toxic organics in wastewater, J. Cleaner Prod., 246 (2020) 118971, doi: 10.1016/j.jclepro.2019.118971.

[5] D.M. EL-Mekkawi, N.A. Abdelwahab, W.A.A. Mohamed, N.A. Taha, M.S.A. Abdel-Mottaleb, Solar photocatalytic treatment of industrial wastewater utilizing recycled polymeric disposals as TiO_2 supports, J. Cleaner Prod., 249 (2020) 119430, doi: 10.1016/j.jclepro.2019.119430.

[6] H.B. He, Z.Z. Luo, C.L. Yu, Embellish zinc tungstate nanorods with silver chloride nanoparticles for enhanced photocatalytic, antibacterial and antifouling performance, Colloids Surf., A, 613 (2021) 126099, doi: 10.1016/j.colsurfa.2020.126099.

[7] M. Martín-Sómer, C. Pablos, A. de Diego, R. van Grieken, Á. Encinas, V.M. Monsalvo, J. Marugán, Novel macroporous 3D photocatalytic foams for simultaneous wastewater disinfection and removal of contaminants of emerging concern, Chem. Eng. J., 366 (2019) 449–459.

[8] H.B. He, Z.Z. Luo, C.L. Yu, Diatomite-anchored g-C_3N_4 nanosheets for selective removal of organic dyes, J. Alloys Compd., 816 (2020) 152652, doi: 10.1016/j.jallcom.2019.152652.

[9] C. Gong, C.Z. Jiang, Preparation of nickel oxide under magnetic field strengthening conditions and its photocatalytic activity, J. Shenyang Ligong Univ., 39 (2020) 46–51.

[10] C.M. Park, Y.M. Kim, K.H. Kim, D. Wang, C.M. Su, Y.M. Yoon, Potential utility of graphene-based nano spinel ferrites as adsorbent and photocatalyst for removing organic/inorganic contaminants from aqueous solutions: a mini review, Chemosphere, 221 (2019) 392–402.

[11] T. Rasheed, M. Adeel, F. Nabeel, M. Bilal, H.M.N. Iqbal, TiO_2/SiO_2 decorated carbon nanostructured materials as a multifunctional platform for emerging pollutants removal, Sci. Total Environ., 688 (2019) 299–311.

[12] Y. Hendrix, A. Lazaro, Q.L. Yu, H.J.H. Brouwers, Influence of synthesis conditions on the properties of photocatalytic titania-silica composites, J. Photochem. Photobiol., A, 371 (2019) 25–32.

[13] S.L. Wang, S.H. Lin, D.Q. Zhang, G.S. Li, M.K.H. Leung, Controlling charge transfer in quantum-size titania for photocatalytic applications, Appl. Catal., B, 215 (2017) 85–92.

[14] H.B. He, Z.Z. Luo, C.L. Yu, Multifunctional $ZnWO_4$ nanoparticles for photocatalytic removal of pollutants and disinfection of bacteria, J. Photochem. Photobiol., A, 401 (2020) 112735, doi: 10.1016/j.jphotochem.2020.112735.
[15] H.B. He, Z.Z. Luo, Z.Y. Tang, C.L. Yu, Controllable construction of $ZnWO_4$ nanostructure with enhanced performance for photosensitized Cr(VI) reduction, Appl. Surf. Sci., 490 (2019) 460–468.
[16] B. Barrocas, L.D. Chiavassa, M. Conceição Oliveira, O.C. Monteiro, Impact of Fe, Mn co-doping in titanate nanowires photocatalytic performance for emergent organic pollutants removal, Chemosphere, 250 (2020) 126240, doi: 10.1016/j.chemosphere.2020.126240.
[17] J.X. Lu, D.L. Li, Y. Chai, L. Li, M. Li, Y.Y. Zhang, J. Liang, Rational design and preparation of nanoheterostructures based on zinc titanate for solar-driven photocatalytic conversion of CO_2 to valuable fuels, Appl. Catal., B, 256 (2019) 117800, doi: 10.1016/j.apcatb.2019.117800.
[18] S. Rahut, R. Panda, J.K. Basu, Solvothermal synthesis of a layered titanate nanosheets and its photocatalytic activity: effect of Ag doping, J. Photochem. Photobiol., A, 341 (2017) 12–19.
[19] G.G. Liu, K. Han, H.Q. Ye, C.Y. Zhu, Y.P. Gao, Y. Liu, Y.H. Zhou, Graphene oxide/triethanolamine modified titanate nanowires as photocatalytic membrane for water treatment, Chem. Eng. J., 320 (2017) 74–80.
[20] C.C. Tsai, L.C. Chen, T.F. Yeh, H. Teng, In situ Sn^{2+}-incorporation synthesis of titanate nanotubes for photocatalytic dye degradation under visible light illumination, J. Alloys Compd., 546 (2013) 95–101.
[21] Y. Zhang, C. Han, G. Zhang, D. Dionysiou, M. Nadagoudaf, PEG-assisted synthesis of crystal TiO_2 nanowires with high specific surface area for enhanced photocatalytic degradation of atrazine, Chem. Eng. J., 268 (2015) 170–179.
[22] A. Patterson, The Scherrer formula for X-ray particle size determination, Phys. Rev., 56 (1939) 978–982.
[23] V. Lojpur, S. Ćulubrk, M.D. Dramićanin, Ratiometric luminescence thermometry with different combinations of emissions from Eu^{3+} doped $Gd_2Ti_2O_7$ nanoparticles, J. Lumin., 169 (2016) 534–538.
[24] P.K. Kulriya, T. Yao, S.M. Scott, S. Nanda, J. Lian, Influence of grain growth on the structural properties of the nanocrystalline $Gd_2Ti_2O_7$, J. Nucl. Mater., 487 (2017) 373–379.
[25] M. Setvin, X. Shi, J. Hulva, T. Simschitz, G.S. Parkinson, M. Schmid, C. Di Valentin, A. Selloni, U. Diebold, Methanol on anatase TiO_2 (101): mechanistic insights into photocatalysis, ACS Catal., 7 (2017) 7081–7091.
[26] H. Arthur, J. Nethercot, Prediction of Fermi energies and photoelectric thresholds based on electronegativity concepts, Phys. Rev. Lett., 33 (1974) 1088–1091.